Mechanisms of Sound-Induced Opening of the Blood-Brain Barrier

31

O. Semyachkina-Glushkovskaya, D. Bragin, O. Bragina, Y. Yang, A. Abdurashitov, A. Esmat, A. Khorovodov, A. Terskov, M. Klimova, I. Agranovich, I. Blokhina, A. Shirokov, N. Navolokin, V. Tuchin, and J. Kurths

Abstract

The blood-brain barrier (BBB) poses a significant challenge for drug delivery to the brain. The limitations of our knowledge about the nature of BBB explain the slow progress in the therapy of brain diseases and absence of methods for drug delivery to the brain in clinical practice. Here, we show that the BBB opens for high-molecular-weight compounds after exposure to loud sound (100 dB 370 Hz) in rats. The role of stress induced by loud sound and the systemic and molecular mechanisms behind it are discussed in the framework of the BBB. This opens an informative platform for novel fundamental knowledge about the nature of BBB and for the development of a noninvasive brain drug delivery technology.

Keywords

Loud sound · Blood-brain barrier · Mechanisms · Cerebral blood oxygen saturation · Meningeal lymphatic clearance

31.1 Introduction

The blood-brain barrier (BBB) is a highly selective barrier, which controls the penetration of blood-borne agents into the brain or the release of metabolites and ions from the brain tissue to blood. Therefore, the BBB plays a vital role in central nervous system (CNS) health protecting

O. Semyachkina-Glushkovskaya (✉) · A. Abdurashitov · A. Esmat · A. Khorovodov · A. Terskov · M. Klimova · I. Agranovich · I. Blokhina · V. Tuchin
Saratov State University, Saratov, Russia

D. Bragin
Lovelace Biomedical Research Institute, Albuquerque, NM, USA

University of New Mexico School of Medicine, Departments of Neurology and Neurosurgery, Albuquerque, NM, USA

O. Bragina
Lovelace Biomedical Research Institute, Albuquerque, NM, USA

Y. Yang
University of New Mexico, College of Pharmacy, Albuquerque, NM, USA

A. Shirokov
Institute of Biochemistry and Physiology of Plants and Microorganisms, Russian Academy of Sciences, Saratov, Russia

N. Navolokin
Saratov State Medical University, Saratov, Russia

J. Kurths
Saratov State University, Saratov, Russia

Humboldt University, Physics Department, Berlin, Germany

Potsdam Institute for Climate Impact Research, Potsdam, Germany

E. M. Nemoto et al. (eds.), *Oxygen Transport to Tissue XLII*, Advances in Experimental Medicine and Biology 1269, https://doi.org/10.1007/978-3-030-48238-1_31

the brain against pathogens and toxins. Although this protective mechanism is essential for normal functioning of CNS, it also creates a hindrance to the entry of drugs into the brain. In this context, it is not surprising that CNS diseases account for 28% of the total burden of all diseases [1]. This is the reason why approaches for reversible overcoming of the BBB have received significant attention in the last four decades. Currently, over 70 different methods are suggested for overcoming the BBB [2, 3]. Nevertheless, these methods are not widely applied in daily clinical practice for many reasons including invasiveness (e.g., photodynamic opening of the BBB that requires trepanation) [4], challenges in performing (intra-arterial injection of mannitol that usually only a few specialists in clinics can do) [5], limitation of drug concentration (intranasal drug delivery) [6], or small area of treatment (only 1–3 mm at usage of focused ultrasound that opens the BBB with additional use of microbubbles) [7]. All these methods require further studies to improve the reproducibility and technological robustness.

In this study on rats, we demonstrate that a factor such as loud sound, which we can meet in daily life when listening to MP3/MP4 players or at a rock concerts, reversibly opens the BBB to low- and high-molecular-weight molecules. We also discuss mechanisms underlying the sound-related opening of BBB.

31.2 Methods

The experiments were done on four groups: (1) no sound – the control group; 2, 3, and 4–1, 4, and 24 h after sound exposure in freely moving mongrel male rats (250–280 g), respectively; $n = 10$ in each group in all experiments.

To produce loud sound (100 dB, 370 Hz), we used a sound speaker (7A, 12 V, Auto VAZ PJSC, Tolyatti, Russia). The sound exposure was performed using the sequence of 60 s, sound on, and then 60 s – sound off over 2 h.

For quantitative assessment of the BBB permeability, we used (1) fluorescent microscopy for in vivo visualization of extravasation of albumin complex of Evans Blue dye (EBAC, 68.5 kDa, 2 mg/body weight, 1% solution in saline, iv, Sigma-Aldrich) via an optically cleared skull window in anaesthetized rats (2% isoflurane at 1 L/min N_2O/O_2–70:30) [8], (2) a spectrofluorometric assay for ex vivo analysis of EBAC leakage [9], and (3) confocal imaging of extravasation of fluorescein isothiocyanate (FITC)-dextran 70 kDa (FITCD, 1 mg/body weight, 0.5% solution in saline, iv, Sigma-Aldrich).

A custom-made laser speckle contrast imaging (LSCI) system was used to monitor relative cerebral blood flow (rCBF) in the cerebral microvessels and in the sagittal sinus [8, 10]. The blood oxygen saturation (SpO2) in the brain was monitored using a pulse oximeter (model CMS60D, Contec Medical Systems Co., Ltd., Qinhuangdao, China). Oxyhemoglobin saturation is presented as a percentage of HbO2 vs. the total Hb in the blood. LSCI and SpO2 were monitored in the same rats before and at 1h/4h after sound exposure via an optically cleared skull window in anaesthetized rats (2% isoflurane at 1 L/min N_2O/O_2–70:30).

The plasma epinephrine level (ng/ml) was determined using ELISA kits (Abnova, Taiwan) at normal state (before sound), during sound stress (at the last minute (120 min) of sound stress), and in the post-stress period (1h and 4h after sound exposure) in rats ($n = 10$ in each group).

Expression of tight junction (TJ) proteins such as claudin-5 (CLND-5), occludin (Occ), zonula occludens-1 (ZO-1), junctional adhesion molecule (JAM), pericyte marker (NG_2), and lymphatic endothelium (LYVE-1) was evaluated using the standard method of simultaneously combined staining (Abcam protocol) using antibodies for indicated proteins (1:500; Santa Cruz Biotechnology, Santa Cruz, USA) with further confocal microscopy of the rat cerebral cortex or the dura mater (Olympus, Japan).

31.3 Results

31.3.1 Blood-Brain Barrier Opening to High-Molecular-Weight Molecules

In the first step, we demonstrated effects of loud sound on the BBB permeability to EBAC and FITCD in in vivo and ex vivo experiments. Using

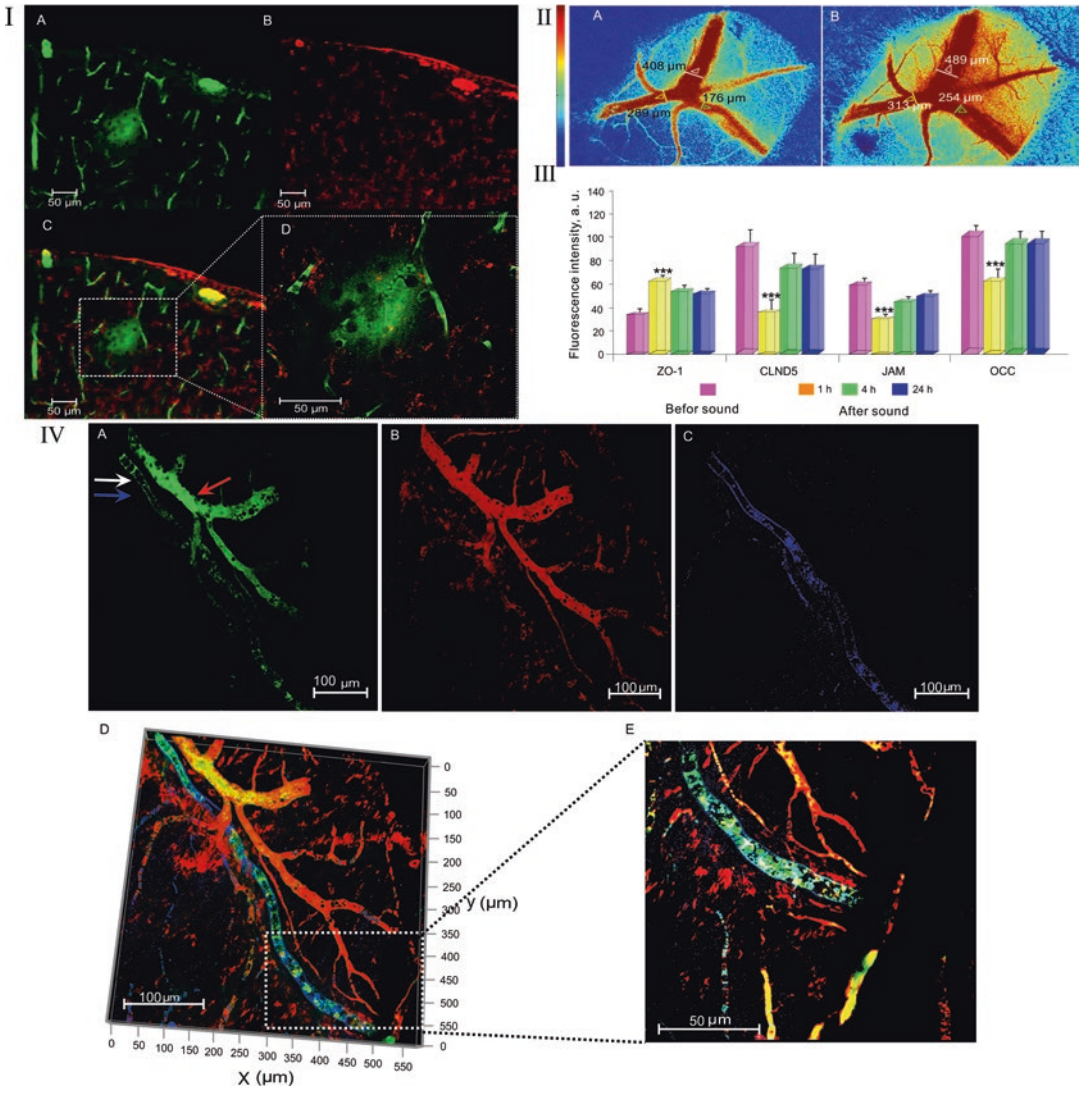

Fig. 31.1 Mechanisms of the sound-induced BBB opening: I – Fluorescent microscopy of EBAC leakage before (A) and 1h after (B) sound exposure. II – Confocal microscopy of the BBB permeability to FITCD before (A–C) and 1h after sound exposure (D–G): A: FITCD is inside of the cerebral vessels (green color), B: the cerebral vessels labelled by pericyte marker NG2 (red color), C: the merged image from A and B, D: FITCD leakage presented as green fluorescence around the cerebral vessel, E: the cerebral vessels labelled by pericyte marker NG2 (red color), F: the merged image from D and E showing FITCD leakage, and G: FITCD leakage at higher magnification from F. III – LSCI of rCBF before (A) and 1h after (B) sound exposure (the time of opening of the BBB). IV – The expression of TJ proteins in the control group (before sound exposure) and 1/4/24 h after sound impact ($n = 10$ for each group): $^{***}p < 0.001$ vs. the control group (before sound). V – The clearance of FITCD from the brain via MLVs after its crossing of the opened BBB: A: the fluorescent signal from FITDC in both anatomical positions of MLV (white arrow) and the cerebral vein (red arrow); B: the cerebral vessels (red color) labelled by NG_2 (pericyte marker); C: MLV (blue color) labelled by LYVE-1 (marker of lymphatic endothelium); D: the merged image from A, B, and C; and E: the same area at higher magnification from D

an in vivo method of real-time fluorescent microscopy, we observed significant EBAC leakage 1h after sound exposure (Fig. 31.1I (A, B)). Afterward, the brains of the same rats were collected for spectrofluorimetric assay and quantitative analysis of the BBB integrity. The results of ex vivo data showed the level of EBAC in the brain tissues was increased 23.1-fold vs. the control group in all rats

Table 31.1 The sound-induced changes in the level of serum epinephrine, rCBF, and SpO_2

	Before sound	After sound			
		0h	1h	4h	24h
rCBF, a.u. (in the sagittal sinus)	0.91 ± 0.05	2.10 ± 0.09 ***	1.84 ± 0.07 **	1.12 ± 0.02	0.97 ± 0.02
rCBF, a.u. (in the cerebral microvessels)	0.37 ± 0.02	0.89 ± 0.04 ***	0.61 ± 0.01 **	0.42 ± 0.03	0. 40 ± 0.01
SpO_2, %	97 ± 3	127 ± 5 *	114 ± 2 *	99 ± 2	97 ± 5
Epinephrine level, ng/ml	5.1 ± 1.9	31.4 ± 5.0 ***	17.0 ± 6.2 **	5.7 ± 2.3	4.9 ± 1.8

***p < 0.001; **p < 0.01; *p < 0.05 vs. the control group (before sound)

(2.61 ± 0.07 vs. 0.11 ± 0.03, $p < 0001$). For qualitative assessment of the BBB permeability, we used confocal imaging of FITCD leakage. Figure 31.1II (D–G) clearly illustrates FITCD extravasation from the cerebral capillaries to the brain tissues 1h after sound exposure. It is important to notice that we did not find an increased BBB permeability to FITCD and EBAC 4h and 24h after sound exposure as well as at the normal state (before sound influences) (Fig. 31.1II (A–C)).

31.3.2 Systemic and Metabolic Responses Induced by Loud Sound

Since loud sound is a stress, we analyzed the general systemic and metabolic stress responses such as changes in the plasma level of epinephrine, rCBF, and SpO_2. The results showed that sound exposure was accompanied by significant increase in epinephrine level vs. the basal value (Table 31.1). The sound stress off was associated with slow normalization of hormone level. One hour after sound exposure, when the BBB was opened, the epinephrine level was decreased but continued to be higher compared with the normal state (Table 31.1). When the BBB closed (4h after sound exposure), the level of epinephrine was over the normal value, and it was not changed to the next day.

LSCI data of rCBF demonstrated an increase in rCBF in both venous and microcirculatory levels immediately after sound stress off (Table 31.1). The BBB opening (1h after sound exposure) was associated with a tendency to normalization of rCBF; however, the level of rCBF was significantly elevated compared to the normal state. Figure 31.1III (A, B) illustrates an increase in rCBF in the time of BBB opening (1h after sound exposure) compared with the control group (before sound). The complete normalization of rCBF was observed at the time of BBB closing (4h after sound exposure) and preserved at the normal level in the next day (Table 31.1).

Similar changes were observed in SpO_2. The sound stress was characterized by a significant increase in SpO_2 that then gradually decreased but continued to be higher at the time of BBB opening (1h after sound exposure) and had returned to the normal values by the time of BBB closing (4 h after sound exposure). In the next day after sound effects on the BBB permeability, we did not observe any changes in SpO_2.

31.3.3 Sound-Induced Changes in TJ Machinery

In the next step, we aimed to study the brain expression of TJ such as CLDN-5, Occ, JAM, and ZO-1 at the time of opening of the BBB (1h after sound) and its recovery (4h and 24h after sound) compared with the control group (before sound exposure). Figure 31.1IV shows that the BBB opening was accompanied by a decrease in expression of CLDN-5, Occ, and JAM and by an increase in expression of ZO suggesting the disorganization of TJ assembly with fast restoration of expression of TJ proteins 4h after sound exposure and without any further changes in the BBB integrity.

31.3.4 Sound-Induced BBB Opening Is Associated with Activation of Lymphatic Clearance of Molecules Crossing the Opened BBB

The important question is how the brain recovers after the sound-induced opening of BBB. To answer this question, we studied clearance of FITCD from the brain after its crossing of the opened BBB via the meningeal lymphatic vessels (MLVs), which play a crucial role in the brain recovery and clearance [11]. With this aim, FITCD was injected intravenously at the time of full opening of the BBB (1h after sound) and circulated for 5 min. Afterward, the brains were removed, and the meninges were collected for confocal microscopy analysis. The results presented in Fig. 31.1V clearly show the presence of FITCD in MLVs suggesting rapid clearance of FITCD from the brain after its crossing of the opened BBB via MLVs.

31.4 Conclusions

We show that loud sound reversibly opens the BBB via stress-mediated TJ machinery disorganization that is accompanied by elevation of serum epinephrine level, rCBF, and SpO_2, as well as by meningeal lymphatic clearance of molecules crossing the BBB. Our data are consistent with the hypothesis suggesting an important role of stress in the BBB opening via mechanisms underlying epinephrine-induced enhancement of the BBB permeability including (1) vasodilation of cerebral vessels and widening of TJs, (2) changes of ultrastructure of endothelial cells and astroglial endfeet, and (3) an increase in transport and the pinocytotic activity of endothelial cells [12–17]. This method has a high potential for clinical applications as an easily used, noninvasive, low-cost, labeling-free perspective and completely new approach for the treatment of brain diseases. The fact that loud sound, which we can meet in daily life, opens the BBB is socially important and should be considered in daily life.

Acknowledgments This work was supported by grants from the Russian Science Foundation (20-15-00090): Visualization of the meningeal lymphatics; RFBR 20-015-00308a: SpO2 recording; grant from the RF Governmental grant 075-15-2019-1885: Methods for the BBB opening. DB was supported by NIH R01 NS112808.

References

1. Silberberg D, Anand N, Michels K et al (2015) Brain and other nervous system disorders across the lifespan – global challenges and opportunities. Nature 527(7578):S151–S154
2. Mitragotri S (2013) Devices for overcoming biological barriers: the use of physical forces to disrupt the barriers. Adv Drug Deliv Rev 65:100–103
3. Pandey P, Sharma A, Gupta U et al (2016) Blood brain barrier: an overview on strategies in drug delivery, realistic in vitro modeling and in vivo live tracking. Tissue Barriers 4(1):e1129476
4. Semyachkina-Glushkovskaya O, Kurths J, Borisova E et al (2017) Photodynamic opening of blood-brain barrier. Biomed Opt Express 8(11):5040–5048
5. Kiviniemi V, Korhonen V, Kortelainen J et al (2017) Real-time monitoring of human blood-brain barrier disruption. PLoS One 12(3):e0174072
6. Wu S, Li K, Yan Y et al (2013) Intranasal delivery of neural stem cells: a CNS-specific, non-invasive cell-based therapy for experimental autoimmune encephalomyelitis. J Clin Cell Immunol 4(3). https://doi.org/10.4172/2155-9899.1000142
7. Chu P-C, Chai W-Y, Tsai C-H et al (2016) Focused ultrasound-induced blood-brain barrier opening: association with mechanical index and cavitation index analyzed by dynamic contrast-enhanced magnetic-resonance imaging. Sci Rep 6:33264. https://doi.org/10.1038/srep33264
8. Yisong Q, Yu T, Jianyi X et al (2019) FDISCO: advanced solvent-based clearing method for imaging whole organs. Sci Adv 5(1). https://doi.org/10.1126/sciadv.aau8355
9. Wang H-L, Lai TW (2014) Optimization of Evans blue quantitation in limited rat tissue samples. Sci Rep 4:6588. https://doi.org/10.1038/srep06588
10. Abdurashitov A, Lychagov V, Sindeeva O et al (2015) Histogram analysis of laser speckle contrast image for cerebral blood flow monitoring. Front Optoelectron 8(2):187–194
11. Semyachkina-Glushkovskaya O, Postnov D, Kurths J (2018) Blood–brain barrier, lymphatic clearance, and recovery: Ariadne's thread in labyrinths of hypotheses. Int J Mol Sci 19:3818

12. Johansson B, Martinsson L (1980) The blood-brain barrier in adrenaline-induced hypertension: circadian variations and modification by beta-adrenoreceptor antagonists. Acta Nellrol Scand 62:96–102
13. Murphy V, Johanson C (1985) Adrenergic-induced enhancement of brain barrier system permeability to small nonelectrolytes: choroid plexus versus cerebral capillaries. JCBFM 5:01–12
14. Sarmento A, Borges N, Azevedo I (1991) Adrenergic influences on the control of blood-brain barrier permeability. Naunyn Schmiedeberg's Arch Pharmacol 343(6):633–637
15. Chi O, Wang G, Chang Q, Weisss H (1998) Effects of isoproterenol on blood-brain barrier permeability in rats. Neurol Res 20(3):259–264
16. Akihiko U, Grubb J, Babks W, Sly W (2007) Epinephrine enhances lysosomal enzyme delivery across the blood-brain barrier by up-regulation of the mannose 6-phosphate receptor. PNAS 104(31):12873–12878
17. Santha P, Veszelka S, Hoyk Z, Meszaros M et al (2016) Restrain stress-induced morphological changes at the blood-brain barrier in adult rats. Front Mo Neurosci 8:88. https://doi.org/10.3389/fnmol.2015.00088

32

Multimodal Measurements of Brain Tissue Metabolism and Perfusion in a Neonatal Model of Hypoxic-Ischaemic Injury

Gemma Bale, Ajay Rajaram, Matthew Kewin, Laura Morrison, Alan Bainbridge, Linshan Liu, Udunna Anazodo, Mamadou Diop, Keith St Lawrence, and Ilias Tachtsidis

Abstract

This is the first multimodal study of cerebral tissue metabolism and perfusion post-hypoxic-ischaemic (HI) brain injury using broadband near-infrared spectroscopy (bNIRS), diffuse correlation spectroscopy (DCS), positron emission tomography (PET) and magnetic resonance spectroscopy (MRS). In seven piglet preclinical models of neonatal HI, we measured cerebral tissue saturation (StO_2), cerebral blood flow (CBF), cerebral oxygen metabolism ($CMRO_2$), changes in the mitochondrial oxidation state of cytochrome c oxidase (oxCCO), cerebral glucose metabolism (CMRglc) and tissue biochemistry (Lac+Thr/tNAA). At baseline, the parameters measured in the piglets that experience HI (not controls) were 64 ± 6% StO_2, 35 ± 11 ml/100 g/min CBF and 2.0 ± 0.4 μmol/100 g/min CMRO2. After HI, the parameters measured were 68 ± 6% StO_2, 35 ± 6 ml/100 g/min CBF, 1.3 ± 0.1 μmol/100 g/min $CMRO_2$, 0.4 ± 0.2 Lac+Thr/tNAA and 9.5 ± 2.0 CMRglc. This study demonstrates the capacity of a multimodal set-up to interrogate the pathophysiology of HIE using a combination of optical methods, MRS, and PET.

Keywords

Near-infrared spectroscopy · Diffuse correlation spectroscopy · Metabolism · Hypoxic ischaemic encephalopathy

32.1 Introduction

Hypoxic-ischaemic encephalopathy (HIE) is responsible for a quarter of neonatal deaths globally and is one of the largest causes of preventable childhood disabilities such as cerebral palsy [1]. The injury evolves throughout treatment, so a continuous monitoring of brain tissue health deployed at the cotside is highly desirable. The progression of the brain health during HIE can be

G. Bale (✉) · I. Tachtsidis
Biomedical Optics Research Laboratory, University College London, London, UK
e-mail: g.bale@ucl.ac.u

A. Rajaram · M. Kewin · L. Morrison · L. Liu · U. Anazodo · M. Diop · K. S. Lawrence
Medical Biophysics, Western University, and Lawson Health Research Institute, London, ON, Canada

A. Bainbridge
Medical Physics, University College London Hospital, London, UK

E. M. Nemoto et al. (eds.), *Oxygen Transport to Tissue XLII*, Advances in Experimental Medicine and Biology 1269, https://doi.org/10.1007/978-3-030-48238-1_32

characterised in terms of the metabolism, progressing from a 'latent phase' where metabolism recovers, to normal levels, to 'secondary energy failure' which may cause further injury. The metabolic state after HIE can be measured using proton (^{1}H) magnetic resonance spectroscopy (MRS) [2]. The ^{1}H MRS-derived thalamic Lac/NAA peak area ratio is a robust predictor of neurodevelopmental outcome in babies with HIE and has been used as a surrogate outcome measure in clinical neuroprotection studies of HIE. This metabolic information is vital for prognostication but only gives a snapshot of the cerebral injury at a particular time point, usually after treatment has been completed. Glucose consumption, measured by FDG PET, is valuable but is also non-continuous and requires injection of radioisotopes so is not ideal for neonatal care [3].

Diffuse optics provides a continuous measurement of brain metabolism. Broadband near-infrared spectroscopy (bNIRS) yields information about cerebral haemodynamics (via oxy- and deoxyhaemoglobin: HbO_2 and HHb, respectively), tissue oxygenation (StO_2) and metabolism from cytochrome c oxidase (CCO). CCO is the terminal electron acceptor in the electron transport chain (ETC): the final stage of oxidative metabolism [4]. We have recently shown that the signal is associated with the level of HI injury [5]. Another optical technique, diffuse correlation spectroscopy (DCS), measures an index of cerebral blood flow, which, combined with oxygenation from NIRS and pulse oximetry, measures cerebral metabolic rate of oxygen ($CMRO_2$) [6]. We have recently shown that it is possible to simultaneously measure CBF and CCO [7]; the aim of this study is to demonstrate how through a combination of optics (bNIRS, DCS), FDG PET and MR measurements we can obtain a full description of the haemodynamic, oxygenation and metabolism status of the brain following HI.

32.2 Methods

32.2.1 Animal Model of HI

This study was approved by the Animal Use Subcommittee of the Canadian Council on Animal Care at Western University (London, Ontario). Piglets were anesthetised under 3% isoflurane during preparatory surgery (2% post surgery), tracheotomised and mechanically ventilated on an oxygen-medical air mixture. Incisions were made lateral to the trachea, and vascular occluders were placed around the carotid arteries posterior to the clavicle (In Vivo Metric, CA). Catheters were inserted into an ear vein for injections and into a femoral artery to monitor vitals (SurgiVet, Smiths Medical, MN), as well as to collect arterial blood samples for gas and glucose analyses. SaO_2 was measured via a pulse oximeter attached to the piglet's right forelimb. The bNIRS and DCS emission/detection fibres were secured to the piglet's left brain, avoiding the sagittal sinus, using an in-house 3D-printed probe holder.

The HI insult was induced by first inflating the occluders around the carotid arteries, followed by reducing the inspired oxygen from 21% to 8%. bNIRS and DCS data were acquired continuously throughout the insult, starting 5 minutes prior to carotid clamping to acquire baseline measurements. The real-time DCS flow index was used to confirm successful clamping, i.e. an immediate drop in CBF. Following this confirmation, inspired oxygen concentration was reduced, and the HI insult was maintained for a minimum duration of 10 minutes once the blood flow index reached its nadir. At the end of the HI insult, recovery was initiated by deflating the carotid occluders and returning oxygen supply to baseline levels.

Data were recorded from seven newborn piglets (four female, aged 10–40 hours): severe HI injury was induced in five piglets and there were two controls.

32.2.2 Measurements of Cerebral Metabolism

Cerebral metabolism was assessed by different modalities: bNIRS and DCS continuously before, during and after the HI and MRS and PET after HI.

The optical device has been fully described previously [7] and is described here briefly. Essentially, it is a bNIRS device and a DCS

device which were run synchronously with a system of shutters to avoid crosstalk between them. The bNIRS device consists of a halogen bulb (Ocean Optics HL-2000-HP) and a custom-made spectrometer (iDus Andor camera, Oxford Instruments; P&P Optica, ON, Canada). For the DCS system, the light source was a long coherence length, continuous-wave laser emitting at 785 nm (DL785–100 s, CrystaLaser, NV) and the detector a single-photon counting module (SPCM-AQR4C, Excelitas, QC, Canada). The output of the SPCM was fed into a correlator board (Flex033LQ-1, Correlator.com, NJ) to generate normalised intensity autocorrelation functions.

The continuous recording of bNIRS and DCS data was set on a 14 s cycle, acquiring 12 bNIRS spectra over 3 s, followed by two DCS measurements over the following 10s, with a 0.5 s delay. These measurements were collected continuously before, during and after HI. Ninety min post HI, the DCS data was calibrated by measuring absolute CBF by DCE-NIRS [8]. The DCE-NIRS protocol consisted of a bolus injection of indocyanine green (ICG, 0.1 mg/kg) into a cannulated vein. The CBF was measured by monitoring the cerebral ICG concentration with bNIRS and the time-varying arterial ICG concentration by a dye densitometer attached to a front paw (DDG 2001, Nihon Kohden, Japan).

Magnetic resonance imaging and spectroscopy and FDG PET were performed after the optical monitoring on a 3 T Biograph mMR scanner (Siemens Healthcare). MR scans included measurements of (lactate + threonine)/(NAA + NAAG) (Lac+Thr/tNAA) from the left hemisphere cortex (ant) and thalamus (bas) with proton (^{1}H) MRS (PRESS: TR = 2 s; TE = 135 or 288 ms) (Fig. 32.1).

32.2.3 Data Analysis

bNIRS: The changes in chromophore concentrations (oxCCO, HbO_2 and HHb) were calculated from the measured changes in broadband near-infrared light attenuation using the modified Beer-Lambert law as applied with the UCLn algorithm [4] across 136 wavelengths (771–906 nm) with a fixed differential path length factor of 4.39 (preterm head) and 3 cm optode separation. To measure absolute StO_2, the spectral data were analysed using the solution to the diffusion approximation for a semi-infinite medium [9]. The absorption coefficient was defined as the sum of the three largest chromophores: HHb, HbO_2 and water. Chromophore concentrations and the scattering terms were determined in a series of steps involving fitting the numerical derivatives of the theoretical model (i.e. the analytical solution to the diffusion approximation) to the derivative spectra.

An algorithm was developed to quantify the recovery of Δ[HbT], Δ[HbDiff], Δ[oxCCO], StO_2 and CBF 1 hour after HI. Data at baseline and recovery were averaged over a 1 min window to calculate the recovery fraction of each signal relative to baseline. All the measurements were normalised against the nadir point:

$$\text{Recovery Fraction}\left(\text{RF}\right) = \frac{\text{Recovery} - \text{Nadir}}{\text{Baseline} - \text{Nadir}} \times 100\%$$

MRS data were analysed using Tarquin [10]. The fitted amplitudes of Lac and Thr were combined because they are not resolvable in in vivo spectra [11].

32.3 Results

Measured attenuation spectra and autocorrelation curves from this data set have been previously presented [7]. Figure 32.2 presents an example of the optical signals obtained and the resulting recovery fractions. The full results with all final absolute metabolic variables are shown in Table 32.1. At baseline, the parameters measured in the piglets that experienced HI (not controls) were 64 ± 6% StO_2, 35 ± 11 ml/100 g/min CBF and 2.0 ± 0.4 μmol/100 g/min $CMRO_2$. After HI, the parameters measured were 68 ± 6% StO_2, 35 ± 6 ml/100 g/min CBF, 1.3 ± 0.1 μmol/100 g/min $CMRO_2$, 0.4 ± 0.2 Lac+Thr/tNAA and 9.5 ± 2.0 CMRglc.

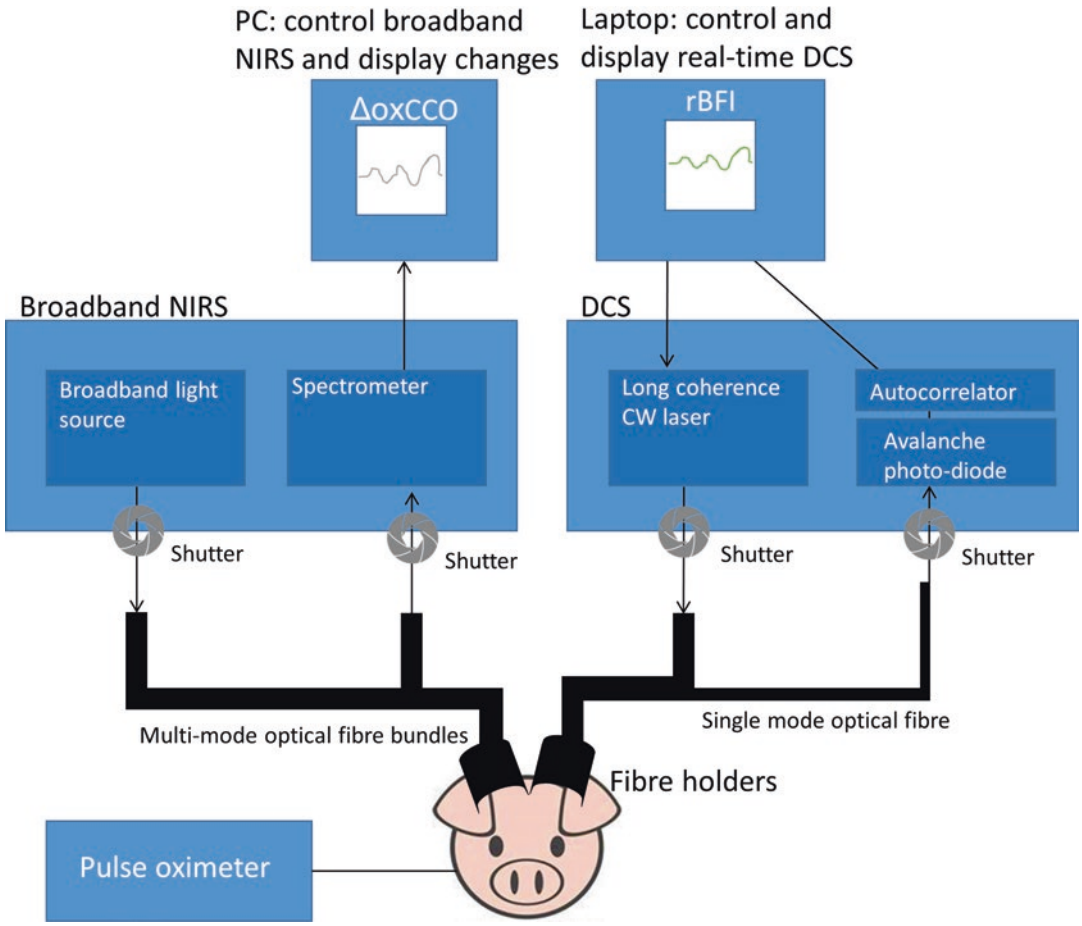

Fig. 32.1 Optical instrumentation for continuous broadband NIRS and DCS measurements

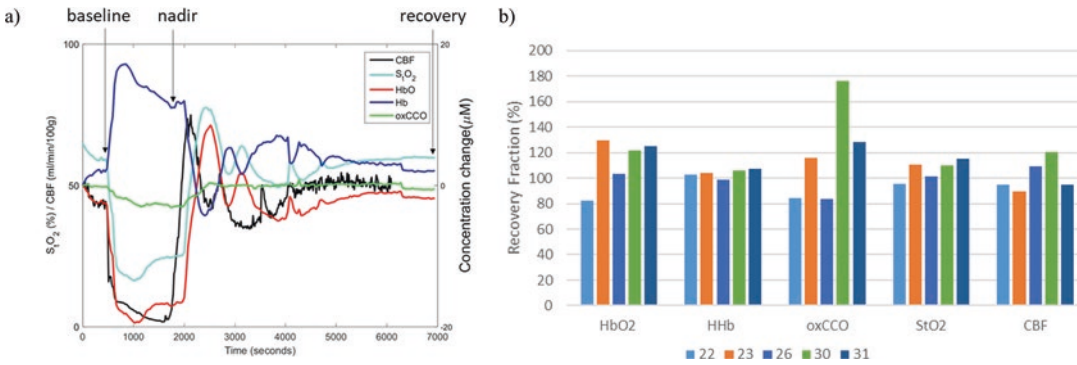

Fig. 32.2 (**a**) Example of optical signals used to calculate recovery fraction (from piglet 26). (**b**) Recovery fractions 1 hour after HI for all optical signals for all HI piglets

Table 32.1 Piglet details and final cerebral measurements. Units: CBF ml/100 g/min, $CMRO_2$ μmol/100 g/min, MRS is Lac+Thr/total NAA and CMRglc μmol/100 g/min. MRS data is missing in some anatomical locations for some animals due to low SNR

Pig	Age (hours)	Weight (kg)	Sex	HI (mins)	StO_2 (%)	CBF	$CMRO_2$	MRS Ant	MRS Bas	CMRglc
20	12	1.4	F	0	65.2	33.6	1.2		0.04	8.44
22	23	1.2	F	10	70.4	35.7	1.2		0.11	8.58
23	10	1.6	M	20	71.7	39.2	1.4		0.57	7.04
26	24	1.5	M	20	64.1	42.0	1.2	0.24	0.35	13.20
28	28	1.9	F	0	45.2	45.5	3.9	0.20	0.29	13.72
30	20	1.8	M	20	75.4	30.8	1.4	0.37	0.39	9.58
31	40	1.7	F	20	59.0	26.6	1.3	0.45		9.10

32.4 Discussion

In this work, we have demonstrated the ability of optical monitoring (bNIRS and DCS) to obtain metabolic information aligned with ^{1}H MRS and FDG PET in a piglet model of HIE. Further, due to the non-invasive, cotside nature of the optical devices, we highlight the potential for continuous measurements of metabolism. The measured parameters are aligned with those obtained by another device working alone; Kaynezhad et al. observed similar changes in HbO_2, HHb and oxCCO during a piglet model of HI [12], and the BFI changes are comparable to those obtained by Rajaram et al. [7].

The recovery fractions obtained with bNIRS and DCS showed that all signals recovered to around 100%, showing that the brain was able to recover to normal levels of oxygenation and metabolism after the insult suggesting that the injury was mild [13]. These optical measures agree with the results from the MR-PET which shown little difference in the recovered metabolic parameters between the control animals and the animals who experienced HI. This may be due to the measurements (both optical and MR-PET) being obtained within the first few hours post HI when the piglets are likely to be in the 'latent phase' of HIE.

This is one of the limitations of this study. Other limitations include the low number of animals involved due to technical issues with the multimodal monitoring which restricts our ability to perform statistical analysis at this stage. Future work includes increasing the number of animals studied and increasing the time between insult and final measurement to capture the metabolic decline during secondary energy failure.

Acknowledgements This research was funded by the Wellcome Trust, grant 104580/Z/14/Z, and an operating grant from the Canadian Institutes of Health Research (St Lawrence).

References

1. Chalak LF, Tian F, Tarumi T, Zhang R (2016) Cerebral hemodynamics in asphyxiated newborns undergoing hypothermia therapy: pilot findings using a multiple-time-scale analysis. Pediatr Neurol 55:30–36
2. Mitra S et al (2019) Proton magnetic resonance spectroscopy lactate/N-acetylaspartate within 2 weeks of birth accurately predicts 2-year motor, cognitive and language outcomes in neonatal encephalopathy after therapeutic hypothermia. Arch Dis Child Fetal Neonatal Ed 104(4):F424–F432
3. Thorngren-Jerneck K et al (2001) Cerebral glucose metabolism measured by positron emission tomography in term newborn infants with hypoxic ischemic encephalopathy. Pediatr Res 49(4):495–501
4. Bale G, Elwell CE, Tachtsidis I (2016) From Jöbsis to the present day: a review of clinical near-infrared spectroscopy measurements of cerebral cytochrome-c-oxidase. J Biomed Opt 21(9):091307
5. Bale G et al (2019) Oxygen dependency of mitochondrial metabolism indicates outcome of newborn brain injury. J Cereb Blood Flow Metab 39(10):2035–2047
6. Durduran T, Choe R, Baker WB, Yodh AG (2010) Diffuse optics for tissue monitoring and tomography. Reports Prog Phys 73(7):076701
7. Rajaram A et al (2018) Simultaneous monitoring of cerebral perfusion and cytochrome c oxidase by combining broadband near-infrared spectroscopy and diffuse correlation spectroscopy. Biomed Opt Express 9(6):2588–2603

8. Cooper JA et al (2011) Continuous monitoring of absolute cerebral blood flow by near-infrared spectroscopy during global and focal temporary vessel occlusion. J Appl Physiol 110(6):1691–1698
9. Yeganeh HZ, Toronov V, Elliott JT, Diop M, Lee T-Y, Lawrence KS (2012) Broadband continuous-wave technique to measure baseline values and changes in the tissue chromophore concentrations. Biomed Opt Express 3(11):2761–2770
10. Wilson M, Reynolds G, Kauppinen RA, Arvanitis TN, Peet AC (2011) A constrained least-squares approach to the automated quantitation of in vivo (1)H magnetic resonance spectroscopy data. Magn Reson Med 65(1):1–12
11. Kreis R, Hofmann L, Kuhlmann B, Boesch C, Bossi E, Hüppi PS (2002) Brain metabolite composition during early human brain development as measured by quantitative in vivo 1H magnetic resonance spectroscopy. Magn Reson Med 48(6):949–958
12. Kaynezhad P et al (2019) Quantification of the severity of hypoxic-ischemic brain injury in a neonatal preclinical model using measurements of cytochrome-c-oxidase from a miniature broadband-near-infrared spectroscopy system. Neurophotonics 6(04):1